Bozok Journal of Science
Volume 3, No 2, Page 89-104 (2025)
Research Article DOI:10.70500/bjs.1808730

Exploring the Quantum Coherence in Heisenberg Spin Chains and Kaplan–Shekhtman–Entin-Wohlman–Aharony Interaction

Durgun DURAN[1*]

[1]Yozgat Bozok University, Faculty of Science and Letters, Department of Physics, 66100, Yozgat, Türkiye

[*]Correspondence: durgun.duran@bozok.edu.tr

Received: 22.10.2025 Accepted: 13.11.2025 Final Version: 20.11.2025

Abstract
A general property of quantum coherence is its non-increasing behavior during any incoherent quantum operation, such as an incoherent quantum channel in a noisy environment. We address that thermal coherence can mitigate these losses by offering relative improvements for different quantum models considering the ferromagnetic and antiferromagnetic properties. It is possible to obtain the thermal coherence of density operators obtained by the actions of the Hamiltonians, even for higher temperatures and certain values of the other parameters compared to other models. By adjusting the parameters, it is maximized such that the state of the output is maximally coherent. These make it possible to create maximal coherence in realizing any quantum information task in a noisy environment.

Keywords: Quantum Coherence, DM interaction, KSEA interaction, Heisenberg models

1. INTRODUCTION

One of the essential characteristics of quantum systems is their ability to exist in linear superpositions of several physical states, in which this quantum phenomenon is called quantum superposition. Quantum coherence, like quantum entanglement and other quantum correlations, is a physical resource (Baumgratz, et.al. 2014; Sashki, et.al. 2014; Aberg, 2014; Rana, et.al. 2016; Streltsov, et.al. 2017) that derives from superposition.

It is an intrinsic feature of an individual quantum system, describing the capacity of a quantum state to preserve its superposition and entanglement despite interactions and thermalization effects. In contrast, quantum correlations generally refer to the interconnections that exist between distinct quantum systems or different degrees of freedom. Quantum coherence is at the center of various quantum properties, such as quantum information processing (Meyer and Wallach, 2002; Bagan, et.al. 2016; Jha, et.al. 2016; Kammerlander and Anders, 2016), quantum optics (Sudarshan, 1963; Glauber, 1963; Mandel and Wolf, 1995), quantum metrology (Giovannetti, Lloyd and Maccone, 2004, 2011; Demkowicz-Dobrzański and Maccone, 2014), quantum biology (Plenio and Huelga, 2008; Lloyd, 2011; Li, et.al. 2012; Huelga and Plenio, 2013; Lambert, et.al. 2013), nanoscale and quantum thermodynamics (Narasimhachar and Gour, 2015; Lostaglio, Jennings and Rudolph, 2015; Lostaglio et.al. 2015; Gour, et.al. 2015; Korzekwa, et.al. 2016), quantum algorithms (Gershenfeld and Chuang, 1997; Chuang, et.al. 1998), quantum supremacy (Harrow and Montanaro, 2017), quantum game theory (Meyer, 1999; Eisert, et.al. 1999; Anand and Benjamin, 2015), which in turn are some of the most important applications of quantum physics, quantum information, and computational science. Recently, there has been a lot of effort to quantify coherence as a resource theory (Baumgratz, et.al. 2014), inspired by the resource theory of entanglement (Plenio and Virmani, 2007; Horodecki, et.al. 2009). Many properties of quantum coherence have been investigated using these coherence measures, including the relationship between quantum coherence and quantum correlations (Streltsov, et.al. 2015; Ma, et.al. 2016; Radhakrishnan, et.al. 2016; Radhakrishnan, et.al. 2017; Yao, et.al. 2015; Xi, et.al. 2015; Duran 2020, 2022; Duran et.al. 2025, Türkmen et.al. 2025) the fact that quantum coherence is affected by quantum noise (Bromley, et.al. 2015; Zhao, et.al. 2018; Wei, et.al. 2018), the phenomenon of coherence freezing (Yu, et.al. 2016), and quantum uncertainty relations of relative entropies of coherence (Zhang and Li, 2018).

[*] https://orcid.org/0000-0002-9458-3715

Coherence is highly delicate and unavoidably influenced by environmental interactions, as real physical systems cannot be completely isolated from their surroundings. Consequently, generating, maintaining, and controlling quantum coherence in quantum systems is generally a challenging task (Rana et al., 2016; Streltsov et al., 2017). Hence, establishing, sustaining, and protecting quantum coherence plays a vital and noteworthy role in quantum computation and quantum information processing. For these purposes, it is important to analyze and implement the dynamics of quantum coherence for any physical model in a noisy environment.

In the present paper, we investigate different types of Hamiltonians to analyze the dynamics of thermal coherence for two-qubit systems. A comprehensive analysis with these Hamiltonians for thermal coherence will be given using the l_1-norm of coherence. We first begin with the Dzyaloshinskii-Moriya (DM) interaction as a simple and practical model to investigate thermal coherence. The foundations of quantum information and quantum physics are enormously influenced by the effects of spin-orbit coupling on non-classical correlations and coherence. Zhang showed that the DM interaction (Dzyaloshinskii, 1958; Moriya, 1960a, 1960b), resulting from the spin-orbit coupling, can excite the thermal entanglement of the Heisenberg model in both the ferromagnetic and antiferromagnetic cases. Furthermore, the ferromagnetic model is also more effective in realizing quantum teleportation than the antiferromagnetic model, provided there is a DM interaction (Zhang, 2007).

Secondly, the Heisenberg model is a simple operational spin chain model that is used to simulate many physical systems such as nuclear spins (Kane, 1998), quantum dots (Loss and DiVincenzo, 1998; Burkard, et.al. 1999; Trauzettel, et.al. 2007), superconductors (Senthil, et.al. 1999, Nishiyama, et.al. 2007), and optical lattices (Sorensen and Molmer, 1999). Since spin is two-level, the Heisenberg model is ideal for the generation of qubit states. Consequently, this concept has gained attention lately due to the development of solid-state quantum computing. The DM interaction terms are incorporated in this model due to spin-orbit couplings in Radhakrishnan, et. al. (2016).

Thirdly, the Kaplan–Shekhtman–Entin-Wohlman–Aharony (KSEA) interaction constrains the local minimum of quantum correlations (Yurischev, 2020). It represents a symmetric type of exchange interaction, which tends to remain stable over time when compared to the antisymmetric Dzyaloshinskii–Moriya (DM) interaction (Yildirim et al., 1995). Kaplan (1983) and Shekhtman et al. (1992, 1993) emphasized the importance of the symmetric KSEA interaction, noting that it can restore the O(3) symmetry of the isotropic Heisenberg model—something the DM interaction cannot achieve. Therefore, in this study, we incorporate both the KSEA and DM interactions to investigate the behavior of thermal coherence in a two-qubit system under an external magnetic field. The system is assumed to be in thermal equilibrium with a heat bath.

This study is organized as follows. In Sec. 2, the main traits of the quantum coherence that will be used in due course is summarized. The dynamics of thermal coherence for DM interaction and the Heisenberg spin chain models with some special cases are carried out in Sec. 3. Thermal coherence for the Heisenberg XXX chain with x-components of DM and KSEA interactions is mentioned in Sec. 4. We end up with some concluding remarks.

2. QUANTUM COHERENCE

Let $\mathcal{H}$ be a d −dimensional Hilbert space and consider a fixed basis of vectors $\{|i\rangle\}_{i=1}^{d}$ in $\mathcal{H}$. A quantum state ρ is defined incoherent if it can be expressed in the following form

$$\rho = \sum_i \varrho_i \, |i\rangle\langle i|. \tag{1}$$

where ϱ_i are probabilities. For a given basis $\{|i\rangle\}_{i=1}^{d}$, the collection of such states is represented by $\mathcal{I} = \{\rho = \sum_i p_i \, |i\rangle\langle i|\}$.

In recent years, coherence has been regarded as a quantum resource, and a formal framework for its quantification has been established (Baumgratz et al., 2014). In their work, Baumgratz and colleagues proposed a set of criteria that any valid coherence measure C should satisfy:

(1) Non-negativity: $C(\rho) \geq 0$ and $C(\rho) = 0$ if and only if ρ is an incoherent.

(2a) Monotonicity: Coherence should not increase under completely positive and trace-preserving (CPTP) incoherent operations, i.e., $C(\Phi(\rho)) \leq C(\rho)$, for any such operation Φ.

(2b) Strong monotonicity: $\sum_i q_i\, C(\rho_i) \leq C(\rho)$, where $\rho_i = (K_i \rho K_i^\dagger)/q_i$ are post-measurement states and $q_i = Tr\left(K_i \rho K_i^\dagger\right)$, with K_i being incoherent Kraus operators.

(3) Convexity: Coherence should not increase under mixing, meaning that

$$\sum_i p_i\, C(\rho_i) \leq C\left(\sum_i p_i\, \rho_i\right). \tag{2}$$

Next, we describe two commonly used measures of quantum coherence.

The first one is the relative entropy of coherence, which serves as a measure of quantum correlations in a bipartite state represented by the density matrix ρ_{AB} (or simply ρ). It is defined as (Baumgratz, et.al. 2014)

$$C_r(\rho) = S\left(\rho_{diag}\right) - S(\rho), \tag{3}$$

where $S(\rho) = -Tr\rho \log \rho$ denotes the von Neumann entropy of ρ and ρ_{diag} is the diagonal part of ρ in the chosen basis. If λ_i are the eigenvalues of ρ then it can be expressed as $S(\rho) = -\sum_i \lambda_i \log \lambda_i$. Since it depends on the chosen basis, this quantity is not basis-independent. The relative entropy of coherence plays a significant role due to its analogy to the relative entropy of entanglement. It also quantifies the optimal rate at which maximally coherent states can be distilled via incoherent operations in the asymptotic limit of many copies of ρ (Winter and Yang, 2016). Interestingly, experimental determination of $C_r(\rho)$ can be achieved without full quantum state tomography (Yu et al., 2016).

The second measure, which is the focus of this work, is the l_1-norm of coherence defined as (Baumgratz et al., 2014)

$$C_{l_1}(\rho) = \sum_{i \neq j} \left|\rho_{ij}\right|, \tag{4}$$

where ρ_{ij} are the off-diagonal elements of ρ. Like C_r, this quantity depends on the basis choice. However, unlike the relative entropy of coherence, the l_1-norm of coherence currently lacks a known counterpart in the resource theory of entanglement (Streltsov et al., 2015). Analogous to the relative entropy of coherence, the l_1-norm of coherence has an operational interpretation. Suppose Alice holds a state ρ^A with the l_1-norm of coherence $C_{l_1}(\rho^A)$. Bob holds another part of the purified state of ρ^A. With the help of Bob performing local measurements and informing Alice of his measurement outcomes using classical communication, Alice's quantum state will be in one pure state ensemble $\{p_k, |\psi_k\rangle\}$ with the l_1-norm of coherence $\sum_k p_k C_{l_1}(|\psi_k\rangle)$. The l_1-norm of coherence of Alice's state is then increased from $C_{l_1}(\rho^A)$ to $\sum_k p_k C_{l_1}(|\psi_k\rangle)$ since the l_1-norm of coherence is a convex function.

The l_1-norm of coherence is usually easy to evaluate and algebraically manipulate for a given quantum state. The l_1-norm of coherence represents the maximum amount of entanglement that can be generated through incoherent operations acting on a system together with an incoherent ancilla. Moreover, any continuous weak coherence monotone that symmetrically depends on the nonzero off-diagonal elements of a quantum state must be a non-decreasing function of this norm (Zhu et al., 2018). The l_1-norm of coherence is also an important link between different coherence measures and entanglement. For example, the l_1-norm of coherence is equal to the robustness of coherence for qubit states and acts as an upper bound for the robustness of coherence in a high dimensional system (Napoli et.al. 2016). Additionally, the logarithmic l_1-norm of coherence serves as an upper bound for the relative entropy of coherence. For any d-dimensional mixed state, it has been demonstrated that $C_{l_1}(\rho) \geq C_r(\rho)/\log_2 d$ and it has been conjectured that $C_{l_1}(\rho) \geq C_r(\rho)$ holds for all quantum states (Rana et al., 2016).

3. DZYALOSHINSKII-MORIYA (DM) INTERACTION

In this section, we shall study the evolution of a thermal state ρ_T formed by different Hamiltonians such as Heisenberg models with DM interaction and then concentrate on the determination of the quantum coherence.

The general Hamiltonian for N-spin Heisenberg model with DM interaction is

$$H_N = \sum_{i=1}^{N-1} \left[J_x \sigma_i^x \otimes \sigma_{i+1}^x + J_y \sigma_i^y \otimes \sigma_{i+1}^y + J_z \sigma_i^z \otimes \sigma_{i+1}^z + \boldsymbol{D} \cdot (\sigma_i \otimes \sigma_{i+1}) \right], \tag{5}$$

where the last term is called the DM interaction arising from spin-orbit couplings. The second-order term known as the Γ tensor is induced by the spin-orbit coupling in addition to the DM interaction (Shekhtman et.al. 1992; Gangadharaiah et.al. 2008; Milivojevic, 2018). This term is neglected in this paper. As a result, only the first-order adjustment of the spin-orbit interaction is valid for this paper. The real parameters J_k $(k = x, y, z)$ denote the symmetric exchange spin-spin interactions, D is the antisymmetric DM exchange interaction or vector coupling and $\sigma_i^{x,y,z}$ are Pauli spin operators on the site i. The system's ferromagnetic and antiferromagnetic properties are represented by the negative and positive J_k, respectively. If $J_x = J_y \neq J_z$, this system is called Heisenberg XXZ model with DM interaction.

3.1 Two-qubit Hesienberg XXX Model

We first consider two-qubit Heisenberg XXX model $H_{N=2} \equiv H_{DM}$ that corresponds to $J_x = J_y = J_z = J$. In this model, the eigenvalues (spectrum) and the corresponding normalized eigenvectors of the Hamiltonian H_{DM} from Eq. (5) are obtained as

$$\lambda_1 = \frac{J}{2}, \qquad |\Psi_1\rangle = |00\rangle, \qquad \lambda_3 = J\sqrt{1+D^2} - \frac{J}{2}, \qquad |\Psi_3\rangle = |+\rangle, \tag{6a}$$

$$\lambda_2 = \frac{J}{2}, \qquad |\Psi_2\rangle = |11\rangle, \qquad \lambda_4 = -J\sqrt{1+D^2} - \frac{J}{2}, \qquad |\Psi_4\rangle = |-\rangle, \tag{6b}$$

where $|\pm\rangle = \left(|01\rangle \pm e^{-i\theta}|10\rangle\right)/\sqrt{2}$ and $\theta = \tan^{-1} D$. Taking the Boltzmann constant $k_B = 1$ and $\beta = 1/k_B T$, the density matrix of the Heisenberg model in the thermal equilibrium as a function of temperature T can be found by

$$\rho_T = \frac{1}{Z} e^{-\beta H_{DM}} = \frac{1}{Z} \sum_{i=1}^{4} \lambda_i |\Psi_i\rangle\langle\Psi_i|, \tag{7}$$

where $Z = Tr\left(e^{-\beta H_{DM}}\right)$ is the partition function and λ_i's are the eigenvalues of H_{DM}. The non-zero elements of ρ_T are calculated in the two-qubit standard basis $\{1 \equiv |00\rangle, 2 \equiv |01\rangle, 3 \equiv |10\rangle, 4 \equiv |11\rangle\}$

$$\rho_{11} = \rho_{44} = \frac{1}{Z} e^{-\beta J/2}, \qquad \rho_{22} = \rho_{33} = \frac{1}{Z} e^{\beta J/2} \cosh\left(\frac{\beta\delta}{2}\right), \qquad \rho_{23} = \rho_{32}^* = -\frac{1}{Z} e^{\beta J/2} \cosh\left(i\theta + \frac{\beta\delta}{2}\right), \tag{8}$$

and the partition function Z is found to be

$$Z = Tr(e^{-\beta H_{DM}}) = 2e^{-\beta J/2} \left[1 + e^{-\beta J} \cosh\left(\frac{\beta\delta}{2}\right)\right], \tag{9}$$

with $\delta = 2J\sqrt{1+D^2}$. The Asterix $*$ denotes the complex conjugation in a computational basis.

From Eq.(4), we can now calculate the l_1-norm of coherence for the thermal state ρ_T of the system

$$C_{l_1}(\rho_T) = \frac{1}{|Z|} \sqrt{2} e^{\Re(\beta J)/2} \left| \sqrt{\cos(2\theta) - \cosh(\beta\delta)} \right|. \tag{10}$$

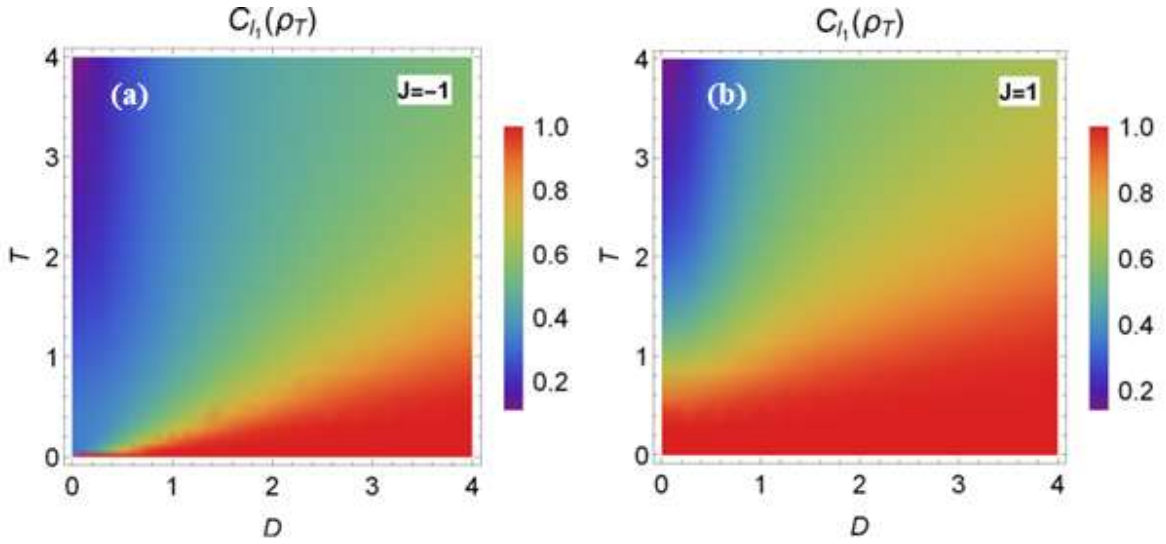

Figure 1. The behavior of the coherence given by Eq. (10) versus temperature T and coupling parameter D for (a) the ferromagnetic $J < 0$ and (b) antiferromagnetic cases > 0 . For both plots, thermal coherence increases with the increasing values of the coupling parameter D and for the antiferromagnetic case compared to the ferromagnetic case, the region of maximum thermal coherence has a wider range. Additionally, both plots are symmetric with respect to the $T = 0$ line, that is thermal coherence also increases for decreasing values of D.

In Fig. 1, we plot the behavior of the quantum coherence of the thermal density matrix ρ_T versus the parameter D and temperature T for the ferromagnetic $J = -1$ and the antiferromagnetic $J = 1$ cases. It is obviously said that in Fig. 1(a) depicted for the ferromagnetic case, the coherence monotonically increases for the increasing values of D at low temperatures. In other words, some relative enhancements of coherence take place in the parameter domain $D < 3.1T$. Furthermore, it attains the maximum values in this domain. For the value of $D = 0$ that corresponds to $\theta = 0$, the coherence reaches its minimum value at the value of temperature T <5. In Fig. 1(b) corresponds to the antiferromagnetic case, the region where the coherence takes place the maximum values is larger than that of Fig. 1(a). In the antiferromagnetic case, higher coherence values are obtained at lower temperatures compared to ferromagnetic ones. Both plots broadly have similar behaviors and are symmetric concerning to the line $D = 0$.

3.2 Two-qubit anisotropic Heisenberg XYZ chain with DM interaction

We here focus on the dynamics of thermal coherence of the two-qubit thermal density matrices ρ_T corresponds to the two different assumptions of the components of the antisymmetric DM exchange interaction D, namely, the cases $D_x = D_y = 0$ and $D_x = D_z = 0$. The case of $D_y = D_z = 0$ is not presented in this paper because all calculations are very similar to the case of $D_x = D_z = 0$. In the first case, the Hamiltonian given by Eq. (5) reduces to

$$H_1 = J_x\sigma_1^x \otimes \sigma_2^x + J_y\sigma_1^y \otimes \sigma_2^y + J_z\sigma_1^z \otimes \sigma_2^z + \boldsymbol{D} \cdot (\sigma_1 \otimes \sigma_2). \tag{11}$$

We first consider the case $D_x = D_y = 0$ and calculate thermal coherence for the corresponding thermal density matrix ρ_T. In this case, the eigenvalues and corresponding normalized eigenvectors for the Hamiltonian H_1 are written as follows

$$\lambda_1 = J_x - J_y + J_z, \quad |\Phi_1\rangle = \frac{1}{\sqrt{2}}(|00\rangle + |11\rangle), \quad \lambda_2 = -J_x + J_y + J_z, \quad |\Phi_2\rangle = \frac{1}{\sqrt{2}}(|00\rangle - |11\rangle) \tag{12a}$$

$$\lambda_3 = -J_z + \xi, \quad |\Phi_3\rangle = \frac{1}{\sqrt{2}}(|01\rangle + e^{i\varphi}|10\rangle), \quad \lambda_4 = -J_z - \xi, \quad |\Phi_4\rangle = \frac{1}{\sqrt{2}}(|01\rangle - e^{i\varphi}|10\rangle) \tag{12b}$$

with

$$\xi = \sqrt{4D_z^2 + (J_x + J_y)^2}, \qquad \varphi = \tan^{-1}\left(-\frac{2D_z}{J_x + J_y}\right). \tag{13}$$

Then, the thermal density matrix ρ_T in this case becomes

$$\rho_T = \frac{1}{Z_1} e^{-\beta H_1} = \begin{pmatrix} a & 0 & 0 & b \\ 0 & c & d & 0 \\ 0 & d^* & c & 0 \\ b & 0 & 0 & a \end{pmatrix}, \tag{14}$$

where the nonzero matrix elements of the density matrix ρ_T in two-qubit computational basis

$$a = \frac{1}{Z_1} e^{-\beta J_z} \cosh\left[\beta\left(J_x - J_y\right)\right], \qquad b = -\frac{1}{Z_1} e^{-\beta J_z} \sinh\left[\beta\left(J_x - J_y\right)\right], \tag{15a}$$

$$c = \frac{1}{Z_1} e^{\beta J_z} \cosh(\beta\xi), \qquad d = -\frac{1}{Z_1} \frac{\left(J_x + J_y + 2iD_z\right)}{\xi} e^{\beta J_z} \sinh(\beta\xi), \tag{15b}$$

with the partition function

$$Z_1 = 2e^{-\beta J_z} \cosh\left[\beta\left(J_x - J_y\right)\right] + 2e^{\beta J_z} \cosh(\beta\xi). \tag{16}$$

The l_1-norm of coherence for the thermal density matrix given by Eq. (14) from Eq. (4) as

$$C_{l_1}(\rho_T) = \frac{1}{|Z_1|} \sqrt{2} e^{-\Re(\beta J_z)} \left\{ e^{2\Re(\beta J_z)} |\sinh(\beta\xi)| + \left| \sinh\left[\beta\left(J_x - J_y\right)\right] \right| \right\}. \tag{17}$$

The behavior of the coherence given by Eq. (17) is plotted in Fig. 2 versus the temperature T and D_z for antiferromagnetic $J_k > 0$ and ferromagnetic cases $J_k < 0$. In Fig. 2(a), the coherence attains its maximum values at the small values of temperature T, especially $T < 1{,}6$ regardless of the values of D_z or for all values of D_z. Additionally, the behavior of coherence has mirror symmetry concerning the $D_z = 0$ line. For the ferromagnetic case, for small values of temperature T the coherence attains its maximum values parallel to Fig. 2(a). Furthermore, for both plots coherence never tends to zero for all values of parameters. While the coherence is maximum for very small values of temperature T in the ferromagnetic case, the coherence can be maximized even at higher temperatures in the antiferromagnetic case than in the ferromagnetic case. Therefore, it is noted that it is more likely to increase coherence in the antiferromagnetic conditions in achieving the applications of the quantum information and computation processes.

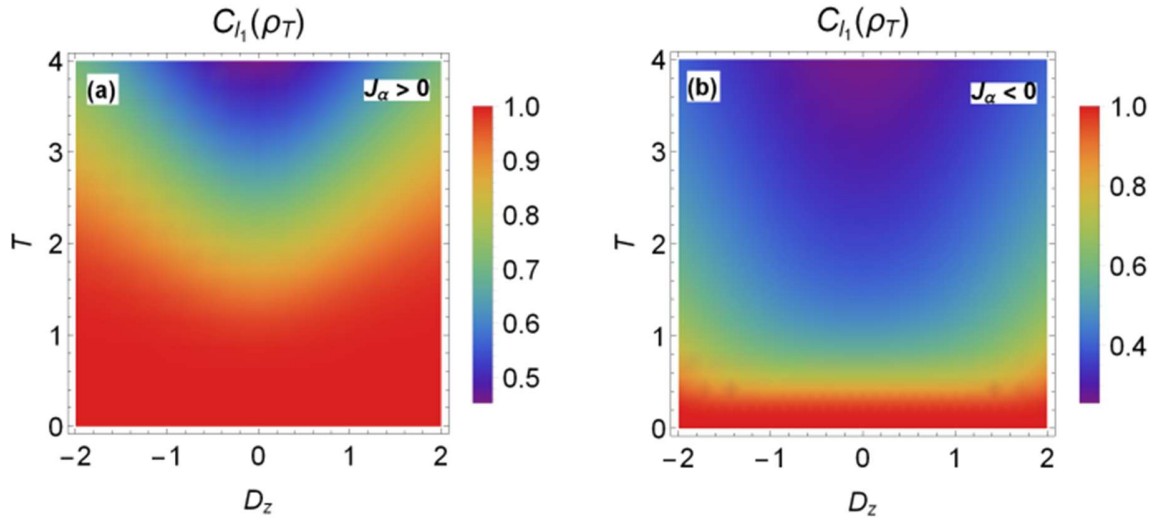

Figure 2. The plots of thermal quantum coherence given by Eq. (17) for the case $D_x = D_y = 0$ (a) antiferromagnetic and (b) ferromagnetic cases that respectively correspond to parameter values $J_x = \pm 1, J_y = \pm 3/2$ and $J_z = \pm 2$.

Secondly, for the case $D_x = D_z = 0$ the eigenvalues and corresponding eigenvectors of the Hamiltonian H_2 in two-qubit computational basis can be found as follows,

$$\lambda_1 = J_y + (J_x - J_z), \qquad |\Upsilon_1\rangle = \frac{1}{\sqrt{2}}(|01\rangle + |10\rangle), \tag{18a}$$

$$\lambda_2 = J_y - (J_x - J_z), \qquad |\Upsilon_2\rangle = \frac{1}{\sqrt{2}}(|00\rangle - |11\rangle), \tag{18b}$$

$$\lambda_3 = -J_y + \eta, \qquad |\Upsilon_3\rangle = \frac{1}{\sqrt{2}}[\sin\phi_1\,(|00\rangle + |11\rangle) - \cos\phi_1\,(|01\rangle - |10\rangle)], \tag{18c}$$

$$\lambda_4 = -J_y - \eta, \qquad |\Upsilon_3\rangle = \frac{1}{\sqrt{2}}[\sin\phi_2\,(|00\rangle + |11\rangle) - \cos\phi_2\,(|01\rangle - |10\rangle)], \tag{18d}$$

where $\eta = \sqrt{4D_y^2 + (J_x + J_z)^2}$ and

$$\phi_1 = \tan^{-1}\left(-\frac{2D_y}{\eta - (J_x + J_z)}\right), \qquad \phi_2 = \tan^{-1}\left(\frac{2D_y}{\eta - (J_x + J_z)}\right). \tag{19}$$

The fact $\cos(\phi_1 - \phi_2) = 0$ guarantees the orthonormal condition of $|\Upsilon_i\rangle$, i.e., $\langle\Upsilon_i|\Upsilon_j\rangle = \delta_{ij}$.

Then, the thermal density matrix ρ_T in this case is obtained as

$$\rho_T = \frac{1}{Z_2}e^{-\beta H_2} = \begin{pmatrix} u & -q & q & s \\ -q & v & p & -q \\ q & p & v & q \\ s & -q & q & u \end{pmatrix}, \tag{20}$$

where the matrix elements of the density matrix ρ_T in two-qubit computational basis

$$u = \frac{1}{2Z_2}\left(e^{-\beta\lambda_3}\sin^2\phi_1 + e^{-\beta\lambda_4}\sin^2\phi_2 + e^{-\beta\lambda_2}\right),$$

$$s = \frac{1}{2Z_2}\left(-e^{-\beta\lambda_3}\sin^2\phi_1 + e^{-\beta\lambda_4}\sin^2\phi_2 + e^{-\beta\lambda_2}\right), \tag{21a}$$

$$v = \frac{1}{2Z_2}\left(e^{-\beta\lambda_1}\cos^2\phi_1 + e^{-\beta\lambda_3}\cos^2\phi_2 + e^{-\beta\lambda_4}\right), \tag{21b}$$

$$p = \frac{1}{2Z_2}\left(e^{-\beta\lambda_1}\cos^2\phi_1 - e^{-\beta\lambda_3}\cos^2\phi_2 - e^{-\beta\lambda_4}\right), \tag{21c}$$

$$q = \frac{1}{2Z_2}\left(e^{-\beta\lambda_3}\sin\phi_1\,\cos\phi_1 + e^{-\beta\lambda_4}\,\sin\phi_2\cos\phi_2\right), \tag{21d}$$

with the partition function Z_2

$$Z_2 = 2e^{-\beta J_y}\cosh[\beta(J_x - J_z)] + 2e^{\beta J_y}\cosh(\beta\eta). \tag{22}$$

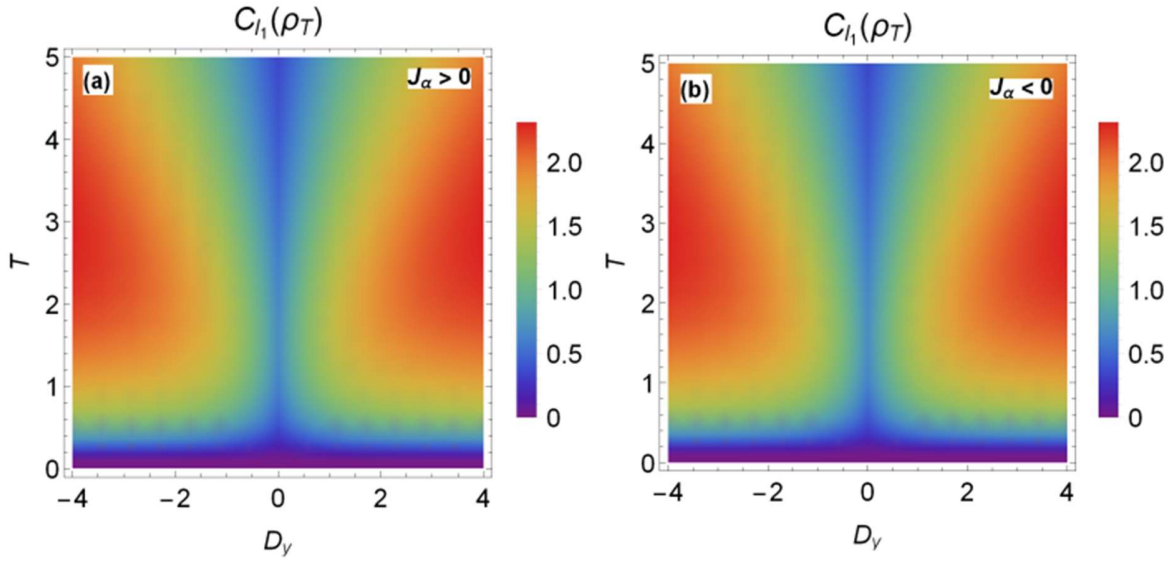

Figure 3. The plots of thermal quantum coherence in the case $D_x = D_z = 0$ for (a) antiferromagnetic and (b) ferromagnetic cases that respectively correspond to $J_x = \pm 1, J_y = \pm 3/2$ and $J_z = \pm 2$.

For this case, the coherence is more complicated and not reported here. The behavior of thermal quantum coherence in the case $D_x = D_z = 0$ is depicted versus temperature T and D_y in Fig. 3 for different values of the parameters J_k. In both antiferromagnetic and ferromagnetic cases, the thermal coherence has similar behavior. Differently from the previous case, the thermal coherence tends to zero for the very small values of temperature T independent of the parameter D_y. Similar to the previous case, it has mirror symmetry concerning the $D_y = 0$ line. On the other hand, the maximum value of coherence is greater here than in the previous case and it takes place $C_{l_1}(\rho_T) = 2$ for relatively small values of temperature T and positive increasing values and negative decreasing values of D_y. It is noted that whether the case is ferromagnetic or antiferromagnetic does not make much difference in terms of coherence, it is important for the achievement of quantum informational and computational processes since the coherence takes a larger value compared to the previous case.

Finally, we consider the behavior of thermal coherence for the multiple DM components and the certain symmetric exchange spin-spin interactions in this section. We choose $D_z = 0$ and $J_x = J_y = J$ for simplicity. In this case, the eigenvalues and corresponding eigenvectors of the Hamiltonian H_{XY} are found to be

$$\lambda_1 = 2J - J_z, \qquad |\Omega_1\rangle = \frac{1}{\sqrt{2}}(|01\rangle + |10\rangle), \tag{23a}$$

$$\lambda_2 = J_z, \qquad |\Omega_2\rangle = \frac{1}{\sqrt{2}}\left(\sqrt{\frac{D_{xy}^*}{D_x + D_y}}|00\rangle + \sqrt{\frac{D_{xy}}{D_{xy}^*}}|11\rangle\right) \tag{23b}$$

$$\lambda_3 = -J + \zeta, \qquad |\Omega_3\rangle = \frac{1}{N_3}\left[-2D_{xy}^*|00\rangle + 2D_{xy}|11\rangle - i\left(J + J_z - \zeta\right)(|01\rangle - |10\rangle)\right], \tag{23c}$$

$$\lambda_4 = -J - \zeta, \qquad |\Omega_3\rangle = \frac{1}{N_4}\left[-2D_{xy}^*|00\rangle + 2D_{xy}|11\rangle - i\left(J + J_z + \zeta\right)(|01\rangle - |10\rangle)\right], \tag{23d}$$

where $D_{xy} = D_x + iD_y$, $\zeta = \sqrt{4\left(D_x^2 + D_y^2\right) + \left(J + J_z\right)^2}$ and the normalization constants are

$$N_3^2 = 4\zeta[\zeta - (J + J_z)], \qquad N_4^2 = 4\zeta[\zeta - (J + J_z)]. \tag{24}$$

Then, the thermal density matrix ρ_T in this case becomes

$$\rho_T = \frac{1}{Z_3} e^{-\beta H_{XY}} = \begin{pmatrix} u_1 & u_3 & -u_3 & u_4 \\ u_3^* & u_2 & u_5 & u_3 \\ -u_3^* & u_5 & u_2 & -u_3 \\ u_4^* & u_3^* & -u_3^* & u_1 \end{pmatrix}, \tag{25}$$

where the matrix elements are explicitly written as

$$u_1 = \frac{1}{2Z_3}\left(e^{-\beta J_z} + \frac{e^{\beta J_z}}{\zeta}[\zeta \cosh(\beta\zeta) - (J + J_z)\sinh(\beta\zeta)] \right), \tag{26a}$$

$$u_2 = \frac{1}{2Z_3}\left(e^{-\beta(2J - J_z)} + \frac{e^{\beta J_z}}{\zeta}[\zeta \cosh(\beta\zeta) + (J + J_z)\sinh(\beta\zeta)] \right), \tag{26b}$$

$$u_3 = -\frac{1}{2Z_3}\frac{\mathrm{i}D_{xy}^*}{\zeta} e^{\beta J}\sinh(\beta\zeta), \tag{26c}$$

$$u_4 = -\frac{1}{2Z_3}\frac{\mathrm{i}D_{xy}^*}{D_{xy}}\left\{ e^{-\beta J_z} - \frac{e^{\beta J_z}}{\zeta}[\zeta \cosh(\beta\zeta) - (J + J_z)\sinh(\beta\zeta)] \right\}, \tag{26d}$$

$$u_5 = \frac{1}{2Z_3}\left\{ e^{-\beta(2J - J_z)} - \frac{e^{\beta J_z}}{\zeta}[\zeta \cosh(\beta\zeta) + (J + J_z)\sinh(\beta\zeta)] \right\}, \tag{26e}$$

with the partition function

$$Z_3 = 2e^{-\beta J}\cosh[\beta(J - J_z)] - 2e^{\beta J}\cosh(\beta\zeta). \tag{27}$$

Thermal coherence for this case can be calculated as from Eq. (4)

$$C_{l_1}(\rho_T) = \frac{1}{|\zeta Z_3|}\left[8e^{-\Re(\beta J)}|\sinh(\beta\zeta)D| + \left|\zeta e^{-\beta J_z} + \omega_- e^{\beta J_z}\right| + \left|\zeta e^{-\beta(-J + J_z)} - \omega_+ e^{\beta J_z}\right| \right], \tag{28}$$

where $D = \sqrt{D_x^2 + D_y^2}$ and $\omega_\pm = [(J + J_z)\sinh(\beta\zeta) \pm \zeta\cosh(\beta\zeta)]$.

The behavior of the thermal coherence for this case is plotted in Fig. (4) versus temperature T and D for the ferromagnetic case that corresponds to the values of parameters $J = -3$ and $J_z = -1$. Since the coherence diverges for the antiferromagnetic case, its graph is not given here. As can be seen from the plot, the thermal coherence is similar to the previous one and has similar behaviors. The most striking feature here is that for increasing values of D, quantum coherence can be maximized even at high temperatures, and this shows that these models studied are useful for obtaining a quantum resource for the achievement of quantum computation applications and tasks.

For the last two cases studied, corresponding respectively to the conditions $D_x = D_z = 0$ and $D_z = 0, J_x = J_y = J$, thermal states ρ_T have full-rank where their ranks equal the largest possible value for a matrix of the same dimension, which is the lesser of the number of rows and columns. In other words, all matrix elements of thermal states are nonzero. Thermal coherence reaches the values of 2, namely $C_{l_1}(\rho_T) = 2$ for certain values of the parameters, and both ferromagnetic and antiferromagnetic analysis in the former case while it takes place the value of 1 in the latter case. In particular, for the latter case, thermal coherence divergences for all choices of the parameters in the antiferromagnetic analysis. It can be said that thermal coherence is a useful and effective resource in the ferromagnetic regime for achieving quantum information and computational tasks.

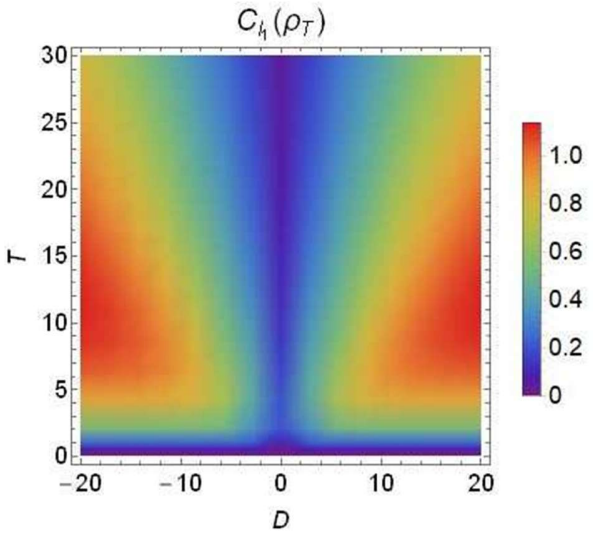

Figure 3. The plot of thermal quantum coherence given by Eq. (28) with respect to temperature T and $D = \sqrt{D_x^2 + D_y^2}$ for the parameters $J = -3$ and $J_z = -1$.

4. HEISENBERG XXX CHAIN WITH X-COMPONENTS OF DM AND KSEA INTERACTIONS

In this section, we take into consideration the N spins of a one-half isotropic Heisenberg XXX chain with an x-component of DM and KSEA interactions for the behavior of thermal coherence. The Hamiltonian can be expressed as

$$H_N = \sum_{i=1}^{N-1} \left[J\left(\sigma_i^x \otimes \sigma_{i+1}^x + \sigma_i^y \otimes \sigma_{i+1}^y + \sigma_i^z \otimes \sigma_{i+1}^z\right) + D_x \Lambda_- + \Gamma_x \Lambda_+ \right] \tag{29}$$

where $\Lambda_\pm = \sigma_i^y \otimes \sigma_{i+1}^z \pm \sigma_i^z \otimes \sigma_{i+1}^y$ and Γ_x denotes the x-component of the KSEA interaction. In two-qubit computational basis, for $N = 2$ the eigenvalues and corresponding eigenvectors of the Hamiltonian H_2 can be written as

$$\lambda_1 = J + 2\Gamma_x, \qquad |\Theta_1\rangle = \frac{1}{2}[(|00\rangle + |11\rangle) - i(|01\rangle + |10\rangle)], \tag{30a}$$

$$\lambda_2 = J + 2\Gamma_x, \qquad |\Theta_2\rangle = \frac{1}{2}[(|00\rangle + |11\rangle) + i(|01\rangle + |10\rangle)], \tag{30b}$$

$$\lambda_3 = -J + \mu, \qquad |\Theta_3\rangle = -\frac{1}{\sqrt{2}}[\sin\theta_1\,(|00\rangle - |11\rangle) + i\cos\theta_1\,(|01\rangle - |10\rangle)], \tag{30c}$$

$$\lambda_4 = -J - \mu, \qquad |\Theta_3\rangle = -\frac{1}{\sqrt{2}}[\sin\theta_2\,(|00\rangle - |11\rangle) - i\cos\theta_2\,(|01\rangle - |10\rangle)], \tag{30d}$$

where $\mu = 2\sqrt{D_x^2 + J^2}$ and

$$\theta_1 = \tan^{-1}\left(\frac{2D_x}{\mu - 2J}\right), \qquad \theta_2 = \tan^{-1}\left(\frac{2D_x}{\mu + 2J}\right). \tag{31}$$

It is straightforward to get the density matrix for the system after we have determined the spectrum of the system. So, when the system is in thermal equilibrium, the density matrix ρ_T can be utilized to represent the system's state at a given temperature T as follows

$$\rho_T = \frac{1}{Z} e^{-\beta H_2} = \begin{pmatrix} a & im & in & c \\ -im & b & d & -in \\ -in & d & b & -im \\ c & in & im & a \end{pmatrix}, \tag{32}$$

where the matrix elements are explicitly written as

$$a = \frac{1}{4Z}\left(e^{-\beta\lambda_1} + e^{-\beta\lambda_2} + 2e^{-\beta\lambda_3}\sin^2\theta_1 + 2e^{-\beta\lambda_4}\sin^2\theta_2\right), \tag{33a}$$

$$b = \frac{1}{4Z}\left(e^{-\beta\lambda_1} + e^{-\beta\lambda_2} + 2e^{-\beta\lambda_3}\cos^2\theta_1 + 2e^{-\beta\lambda_4}\cos^2\theta_2\right), \tag{33b}$$

$$c = \frac{1}{4Z}\left(e^{-\beta\lambda_1} + e^{-\beta\lambda_2} + e^{-\beta\lambda_3}\sin^2\theta_1 - e^{-\beta\lambda_4}\sin^2\theta_2\right), \tag{33c}$$

$$d = \frac{1}{4Z}\left(e^{-\beta\lambda_1} + e^{-\beta\lambda_2} - 2e^{-\beta\lambda_3}\sin^2\theta_1 - 2e^{-\beta\lambda_4}\sin^2\theta_2\right), \tag{33d}$$

$$m = \frac{1}{4Z}\left[-e^{-\beta\lambda_1} + e^{-\beta\lambda_2} + e^{-\beta\lambda_3}\sin^2(2\theta_1) - 2e^{-\beta\lambda_4}\sin^2(2\theta_2)\right], \tag{33e}$$

$$n = \frac{1}{4Z}\left[-e^{-\beta\lambda_1} + e^{-\beta\lambda_2} - e^{-\beta\lambda_3}\sin^2(2\theta_1) + 2e^{-\beta\lambda_4}\sin^2(2\theta_2)\right], \tag{33f}$$

with the partition function Z

$$Z = e^{\beta J}\cosh(\beta\mu) + 2e^{-\beta J}\cosh(2\beta\Gamma_x). \tag{34}$$

For this model, thermal coherence is obtained in compact form as

$$C_{l_1}(\rho_T) = \frac{1}{|Z|} 2(|c| + |d| + 2|m| + 2|n|). \tag{35}$$

The behavior of thermal coherence given by Eq. (35) for the KSEA interaction is plotted in Fig. (5) versus temperature T, x-components of DM and KSEA interactions, that is D_x and Γ_x for the antiferromagnetic and ferromagnetic cases. From Fig. 5(a), thermal coherence increases with the increasing values of the x-component of DM D_x and the small values of temperature T for some certain values of the coupling constants for the spin interaction $J = 2$ and the x-component of the KSEA interaction $\Gamma_x = 2$ in the antiferromagnetic case. It vanishes for the values of the x-component of DM $D_x = 0$ at low temperatures. In Fig. 5(b), thermal coherence reaches its maximum value at low temperatures especially ground state $T = 0$ for the values of the x-component of the KSEA interaction $\Gamma_x = 0$ at the fixed $D_x = 2$ and the same values of J. It is noted that thermal coherence never tends to zero even for different values of parameters. However, it has a lower maximum value contrary to the previous one.

For the ferromagnetic case, from Fig. 5(c) thermal coherence attains its maximum values at low temperatures, especially ground state $T = 0$ like (b) for the values of the other parameters $J = -2$ and $\Gamma_x = 2$. Differently from (b), for the increasing values of D_x approximately $D > 2.7$ thermal coherence increases but never reaches its maximum value. On the other hand, in Fig. 5(d) thermal coherence increases with the increasing values of the parameter Γ_x at low temperatures for the fixed $J = -2$ and $D_x = 2$. Moreover, at low temperatures, it has some values but similar to the previous one never reaches its maximum for $\Gamma_x = 0$ in which the Hamiltonian reduces the DM interaction. In this region, namely $0 < \Gamma_x < 1$, coherence decreases with the increasing values of temperature T independent of the other parameters.

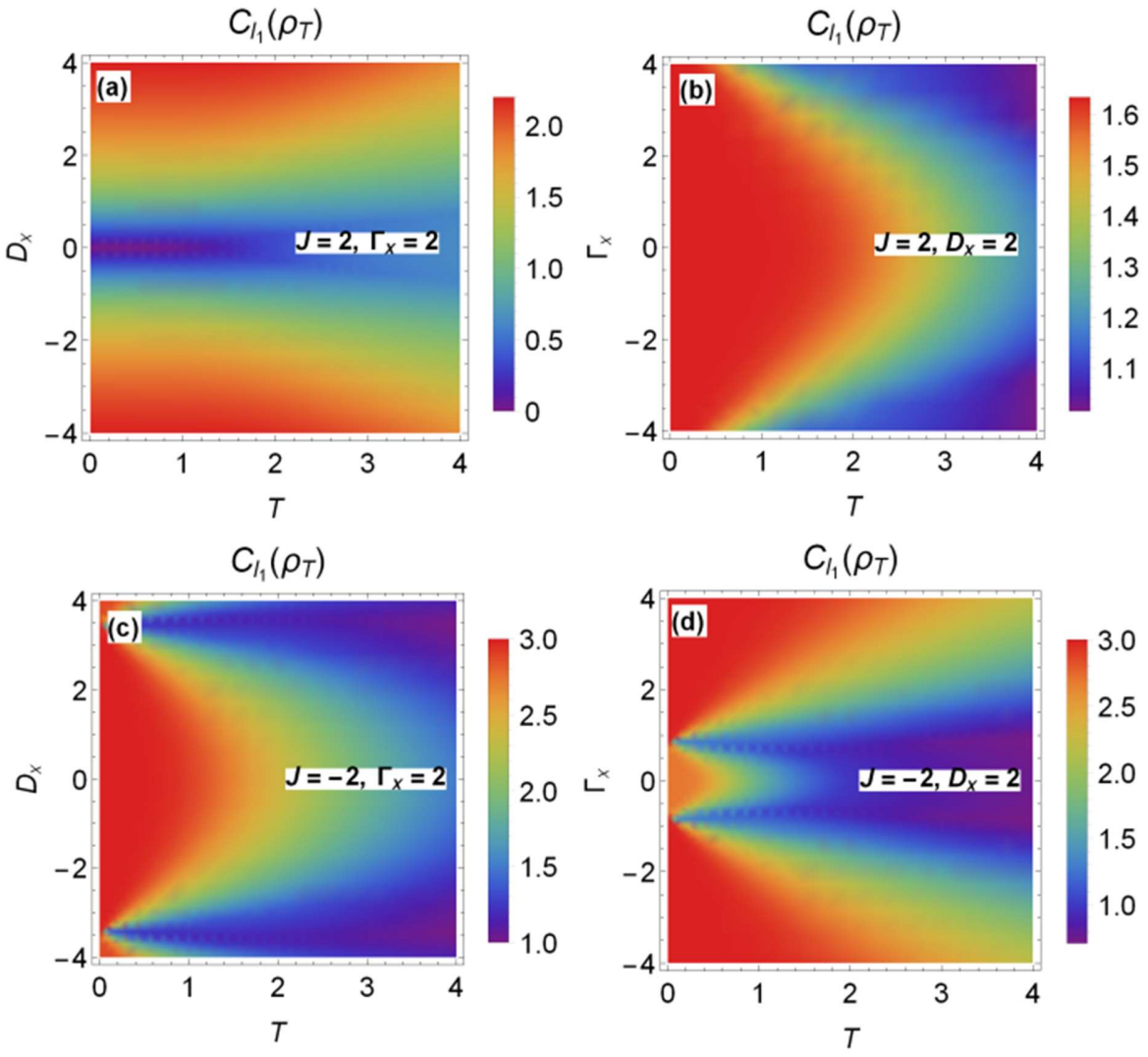

Figure 5. Plots of thermal coherence under the KSEA interaction for the antiferromagnetic and ferromagnetic cases versus the parameters D_x and Γ_x. For the antiferromagnetic case, the thermal coherence symmetrically increases with increasing values of $D_x > 0$ and decreasing values of $D_x < 0$ for low temperatures and the fixed $J = 2$ and $\Gamma_x = 2$ in (a). In (b), the thermal coherence attains its maximum value for low temperatures and small values of Γ_x, especially $\Gamma_x = 0$, for $J = 2$ and $D_x = 2$. For the ferromagnetic case, the situation is reversed with respect to Γ_x and D_x in (c) and (d). Additionally, since the thermal state is maximally coherent thermal coherence takes place the maximum value it can reach.

Parallel to the previous case, for all plots, since thermal states have full rank, it is observed that $C_{l_1}(\rho_T) = 3$, because thermal state is maximally coherent. It is concluded that thermal coherence may be kept at high values with the appropriate choice of parameters in achieving the applications of the quantum information and computation tasks for both ferromagnetic and antiferromagnetic cases, especially ferromagnetic ones.

5. CONCLUSION

In this paper, we have studied the behavior of thermal coherence for the thermal state constructed by different quantum models such as DM interaction, Heisenberg chains and KSEA interaction. Thermal coherence is inclusively and comparatively computed for all models except the last one, overwhelming the thermalization effects both in the ferromagnetic and in antiferromagnetic regions. In the antiferromagnetic case, the region where the maximum values of thermal coherence are obtained is wider than in the ferromagnetic case

for the two-qubit Heisenberg XXX chain, in general for other models as well. Thermal coherence also increases with the increasing values of the antisymmetric DM exchange interaction parameter D.

On the other hand, to a more or lesser degree, the temperature T, the x-components of the DM, and the KSEA interactions may all influence how complex the states are. The results also suggest that the ferromagnetic chain or the high-temperature domains can yield the separability of the states. For large values of the x-components of the DM and KSEA interactions, or in the antiferromagnetic phase, the entanglement of the states can be produced. Furthermore, it is well known that quantum coherence monotonically decreases under the action of an incoherent quantum channel or any local operation. However, we have observed relative enhancements of coherence for some different Hamiltonians adjusting the parameters. Especially, it can be concluded that thermal state for the antiferromagnetic case is maximally coherent since thermal coherence is equal to 3. In conclusion, we should note that further improvements in thermal coherence are possible with the choice of parameters. It would be interesting to see the thermodynamical properties of the quantum system such as work, quantum thermometry, internal energy and entropy possible for these models and would also make an important contribution to the field of quantum thermodynamics.

ACKNOWLEDGMENT

This work is supported in part by the Scientific and Technological Research Council of Turkey (TUBITAK).

AUTHOR'S CONTRIBUTIONS

All authors contribute equally.

CONFLICTS OF INTEREST

The authors declare that they have no conflict of interest.

RESEARCH AND PUBLICATION ETHICS

The author declares that this study complies with Research and Publication Ethics.

REFERENCES

Åberg, J. (2014). Catalytic coherence. Physical Review Letters, 113(15), 150402.

Anand, N., & Benjamin, C. (2015). Do quantum strategies always win? Quantum Inf. Process. 14(10), 4027-4038.

Bagan, E., Bergou, J. A., Cottrell, S. S., & Hillery, M. (2016). Relations between coherence and path information. Phys. Rev. Lett. 116(16), 160406.

Baumgratz, T., Cramer, M. & Plenio, M. B. (2014). Quantifying coherence. Phys. Rev. Lett. 113(14), 140401.

Bromley, T. R., Cianciaruso, M. & Adesso, G. (2015). Frozen quantum coherence. Phys. Rev. Lett. 114(21), 210401.

Burkard, G., Loss, D. & DiVincenzo, D. P. (1999). Coupled quantum dots as quantum gates. Phys. Rev. B, 59(3), 2070–2078.

Chuang, I. L., Vandersypen, L. M. K., Zhou, X., Leung, D. W. & Lloyd, S. (1998). Experimental realization of a quantum algorithm. Nature, 393(6681), 143–146.

Demkowicz-Dobrzański, R., & Maccone, L. (2014). Using entanglement against noise in quantum metrology. Phys. Rev. Lett. 113(25), 250801.

Duran, D. (2020). Action in Hamiltonian Models Constructed by Yang-Baxter Equation: Entanglement and Measures of Correlation. Chinese Journal of Physics, 68, 426-435.

Duran, D. (2022). Dynamics of the quantum coherence under the concatenation of Yang-Baxter matrix. Quantum Inf. Process., 21(2), 50.

Duran, D., Türkmen, A., Çelebi, G. & Dernek, B. (2025). Dynamics in the Yang-Baxter systems: Thermal quantum coherence and quantum correlations. European Physical Journal Plus, 140(9), 926.

Dzyaloshinskii, I. (1958). A thermodynamic theory of weak ferromagnetism of antiferromagnetics. J. Phys. Chem. Solids, 4(4), 241-255.

Eisert, J., Wilkens, M. & Lewenstein, M. (1999). Quantum games and quantum strategies. Phys. Rev. Lett. 83(15), 3077-3080.

Gangadharaiah, S., Sun, J., Starykh, O.A. (2008). Spin-orbit-mediated anisotropic spin interaction in interacting electron systems. Phys. Rev. Lett. 100, 156402.

Gershenfeld, N. A. & Chuang, I. L. (1997). Bulk spin-resonance quantum computation. Science, 275(5298), 350–356.

Giovannetti, V., Lloyd, S., & Maccone, L. (2004). Quantum-enhanced measurements: Beating the standard quantum limit. Science, 306(5700), 1330.

Giovannetti, V., Lloyd, S., & Maccone, L. (2011). Advances in quantum metrology. Nature Photonics, 5, 222–229.

Glauber, R. J. (1963). The quantum theory of optical coherence. Physical Review, 131(6), 2766.

Gour, G., Müller, M., Narasimhachar, V., Spekkens, R. & Yunger Halpern, N. (2015). The resource theory of informational nonequilibrium in thermodynamics. Physics Reports, 583, 1–58.

Harrow, A. W. & Montanaro, A. (2017). Quantum computational supremacy. Nature, 549(7671), 203–209.

Horodecki, R., Horodecki, P., Horodecki, M. & Horodecki, K. (2009). Quantum entanglement. Rev. Mod. Phys. 81(2), 865–942.

Huelga, S. F., & Plenio, M. B. (2013). Vibrations, quanta and biology. Contemporary Physics, 54(4), 181–207.

Jha, P. K., Mrejen, M., Kim, J., Wu, C., Wang, Y., Rostovtsev, Y. V., & Zhang, X. (2016). Coherence-driven topological transition in quantum metamaterials. Phys. Rev. Lett., 116(16), 165502.

Kammerlander, P., & Anders, J. (2016). Coherence and measurement in quantum thermodynamics. Sci. Rep. 6, 22174.

Kane, B. E. (1998). A silicon-based nuclear spin quantum computer. Nature, 393(6681), 133–137.

Kaplan, T. A. (1983). Single-band Hubbard model with spin-orbit coupling. Z. Phys. B: Condens. Matter, 49(4), 313–317.

Korzekwa, K., Lostaglio, M., Oppenheim, J. & Jennings, D. (2016). The extraction of work from quantum coherence. New J. Phys. 18(2), 023045.

Lambert, N., Chen, Y.-N., Cheng, Y.-C., Li, C.-M., Chen, G.-Y., & Nori, F. (2013). Quantum biology. Nat. Phys. 9(1), 10–18.

Li, C.-M., Lambert, N., Chen, Y.-N., Chen, G.-Y., & Nori, F. (2012). Witnessing quantum coherence: From solid-state to biological systems. Sci. Rep. 2, 885.

Lloyd, S. (2011). Quantum coherence in biological systems. Journal of Physics: Conference Series, 302(1), 012037.

Loss, D. & DiVincenzo, D. P. (1998). Quantum computation with quantum dots. Phys. Rev. A, 57(1), 120–126.

Lostaglio, M., Jennings, D., & Rudolph, T. (2015). Description of quantum coherence in thermodynamic processes requires constraints beyond free energy. Nature Communications, 6, 6383.

Lostaglio, M., Korzekwa, K., Jennings, D., & Rudolph, T. (2015). Quantum coherence, time-translation symmetry, and thermodynamics. Phys. Rev. X, 5(2), 021001.

Ma, J., Yadin, B., Girolami, D., Vedral, V. & Gu, M. (2016). Converting coherence to quantum correlations. Phys. Rev. Lett. 116(16), 160407.

Mandel, L., & Wolf, E. (1995). Optical coherence and quantum optics. Cambridge University Press.

Meyer, D. (1999). Quantum strategies. Phys. Rev. Lett. 82(5), 1052–1055.

Meyer, D., & Wallach, N. (2002). Global entanglement in multiparticle systems. Journal of Mathematical Physics, 43(9), 4273.

Milivojević, M. (2018). Symmetric spin-orbit interaction in triple quantum dot and minimization of spin-orbit leakage in CNOT gate. J. Phys.: Condens. Matter 30, 085302.

Moriya, T. (1960a). New mechanism of anisotropic superexchange interaction. Phys. Rev. Lett. 4(5), 228–230.

Moriya, T. (1960b). Theory of magnetism of NiF_2. Physical Review, 117(3), 635–647.

Napoli, C., Bromley, T.R., Cianciaruso, M., Piani, M., Johnston, N., Adesso, G. (2016). Robustness of Coherence: An Operational and Observable Measure of Quantum Coherence. Phys. Rev. Lett. 116, 150502.

Narasimhachar, V., & Gour, G. (2015). Low-temperature thermodynamics with quantum coherence. Nature Communications, 6, 7689.

Nishiyama, M., Inada, Y. & Zheng, G. (2007). Spin triplet superconducting state due to broken inversion symmetry in Li_2Pt_3B. Phys. Rev. Lett. 98(4), 047002.

Plenio, M. B., & Huelga, S. F. (2008). Dephasing-assisted transport: Quantum networks and biomolecules. New J. Phys. 10(11), 113019.

Plenio, M. B., & Virmani, S. (2007). An introduction to entanglement measures. Quantum Inf. Comput. 7(1–2), 1–51.

Radhakrishnan, C., Parthasarathy, M., Jambulingam, S. & Byrnes, T. (2016). Distribution of quantum coherence in multipartite systems. Phys. Rev. Lett. 116(15), 150504.

Radhakrishnan, C., Parthasarathy, M., Jambulingam, S. & Byrnes, T. (2017). Quantum coherence of the Heisenberg spin models with Dzyaloshinsky-Moriya interactions. Sci. Rep. 7(1), 1.

Rana, S., Parashar, P., & Lewenstein, M. (2016). Trace-distance measure of coherence. Phys. Rev. A, 93(1), 012110.

Sasaki, T., Yamamoto, Y. & Koashi, M. (2014). Practical quantum key distribution protocol without monitoring signal disturbance. Nature, 509(7501), 475.

Senthil, T., Marston, J. B. & Fisher, M. P. A. (1999). Spin quantum Hall effect in unconventional superconductors. Phys. Rev. B, 60(6), 4245-4254.

Shekhtman, L., Aharony, A. & Entin-Wohlman, O. (1993). Bond-dependent symmetric and antisymmetric superexchange interactions in La_2CuO_4. Phys. Rev. B, 47(1), 174-182.

Shekhtman, L., Entin-Wohlman, O. & Aharony, A. (1992). Moriya's anisotropic superexchange interaction, frustration, and Dzyaloshinsky's weak ferromagnetism. Phys. Rev. Lett. 69(5), 836-839.

Sørensen, A. & Mølmer, K. (1999). Spin-spin interaction and spin squeezing in an optical lattice. Phys. Rev. Lett. 83(11), 2274-2277.

Streltsov, A., Adesso, G., & Plenio, M. B. (2017). Colloquium: Quantum coherence as a resource. Rev. Mod. Phys. 89(4), 041003.

Streltsov, A., Singh, U., Dhar, H. S., Bera, M. N. & Adesso, G. (2015). Measuring quantum coherence with entanglement. Phys. Rev. Lett. 115(2), 020403.

Sudarshan, E. C. G. (1963). Equivalence of semiclassical and quantum mechanical descriptions of statistical light beams. Phys. Rev. Lett. 10(7), 277.

Trauzettel, B., Denis, V., Loss, D., Bulaev, D. & Burkard, G. (2007). Spin qubits in graphene quantum dots. Nat. Phys. 3(3), 192–196.

Türkmen, A., Çelebi, G., Dernek, B. & Duran, D. (2025). Quantum thermometry for the Hamiltonians constructed by quantum Yang-Baxter equation. Quantum Inf. Process. 24(1), 2.

Wei, S.-J., Xin, T. & Long, G.-L. (2018). Efficient universal quantum channel simulation in IBM's cloud quantum computer. Sci. China Physics Mech. Astronomy, 61(7), 070311.

Winter, A., Yang, D. (2016) Operational Resource Theory of Coherence. Phys. Rev. Lett. 116,120404.

Xi, Z., Li, Y. & Fan, H. (2015). Quantum coherence and correlations in quantum system. Sci. Rep. 5, 10922.

Yao, Y., Xiao, X., Ge, L. & Sun, C. P. (2015). Quantum coherence in multipartite systems. Phys. Rev. A, 92(2), 022112.

Yildirim, T., Harris, A. B., Aharony, A. & Entin-Wohlman, O. (1995). Anisotropic spin Hamiltonians due to spin-orbit and Coulomb exchange interactions. Phys. Rev. B, 52(14), 10239-10267.

Yu, X.-D., Zhang, D.-J., Liu, C. L. & Tong, D. M. (2016). Measure-independent freezing of quantum coherence. Phys. Rev. A, 93(6), 060303.

Yurischev, M. A. (2020). On the quantum correlations in two-qubit XYZ spin chains with Dzyaloshinsky–Moriya and Kaplan–Shekhtman–Entin-Wohlman–Aharony interactions. Quantum Inf. Process. 19(9), 336.

Zhang, F.-G. & Li, Y. (2018). Quantum uncertainty relations of two generalized quantum relative entropies of coherence. Sci. China Physics Mech. Astronomy, 61(8), 080312.

Zhang, G. F. (2007). Thermal entanglement and teleportation in a two-qubit Heisenberg chain with Dzyaloshinski-Moriya anisotropic antisymmetric interaction. Phys. Rev. A, 75(3), 034304.

Zhao, M.-J., Ma, T. & Ma, Y.-Q. (2018). Coherence evolution in two-qubit system going through amplitude damping channel. Sci. China Physics Mech. Astronomy, 61(2), 020311.

Zhu, H., Hayashi, M. & Chen, L. (2018). Axiomatic and operational connections between the l1-norm of coherence and negativity. Phys. Rev. A 97, 022342.